Excitation and Decay of Electron Acoustic Waves

Francesco Valentini*, Thomas M. O'Neil† and Daniel H. E. Dubin†

*Dipt. di Fisica and INFM, Univ. della Calabria, 87036 Rende, Italy
†Department of Physics, University of California at San Diego, La Jolla, California 92093

Abstract. A particle in cell (PIC) simulation is used to investigate the excitation of electron acoustic waves (EAWs) by a driver electric field and the stability of the EAWs against decay. An EAW is a nonlinear wave with a carefully tailored trapped particle population, and the excitation process must create the trapped particle population. For a nearly collisionless plasma, successful excitation occurs when a relatively low amplitude driver that is spatially and temporally resonant with the EAW is applied for a sufficiently long time (many trapping periods). The excited EAW rings at nearly constant amplitude long after the driver is turned off, provided the EAW has the largest wavelength that fits in the simulation domain. Otherwise, the excited EAW decays to a longer wavelength EAW. In phase space, this decay to longer wavelength appears as a tendency of the vortex-like trapped particle populations to merge.

Keywords: <Enter Keywords here>
PACS: 52.65.Ff; 52.65.Rr; 52.35.Fp; 52.35.Mw; 52.35.Sb

INTRODUCTION

In 1991, Hollway and Dorning [1] noted that certain nonlinear wave structures can exist in a plasma even at low amplitude. They called these waves electron-acoustic waves (EAW) since the dispersion relation is of the acoustic form (i.e., $\omega = 1.31kv_{th}$ for small k). Here, ω is the angular frequency of the wave, k the wave number, and v_{th} the thermal velocity of the plasma electrons.

Within linear theory, an EAW would be heavily Landau damped, since the wave phase velocity is comparable to the electron thermal velocity [2]. However, the EAW is a Bernstein-Green-Kruskal nonlinear mode (BGK mode) [3] with electrons trapped in the wave troughs. Because of the trapped electrons, the distribution of electron velocities is effectively flat at the wave phase velocity, and this turns off Landau damping.

These waves can be constructed even at low amplitude by carefully tailoring the trapped particle distribution. However, the importance of the waves as elementary excitations of the plasma, such as Langmuir waves (LW), depends on the extent to which they are excited by general perturbations and drives applied to the plasma, and the extent to which they are stable against decay to other modes. Because EAWs are intrinsically nonlinear structures, one expects that parametric decay instabilities are possible.

A simple argument shows that the waves can be excited by a sudden (or initial) perturbation only at large amplitude. We assume here that the trapped particle distribution does not exist initially, but forms dynamically as the wave evolves. For a wave electric field $E\ \sin(kx-\omega t)$, the time to form the trapped particle distribution is approximately the period for trapped particles to oscillate in the trough of the wave, $\tau_t = 2\pi\sqrt{m/(eEk)}$, where e and m are the electron charge and mass, respectively [4]. The wave is killed by

Landau damping before the trapped particle distribution can form unless $\gamma_L \tau_t < 1$, where γ_L is the linear Landau damping rate [2]. For a wave with phase velocity comparable to the thermal velocity $(\omega/k \sim v_{th})$, the Landau damping rate is comparable to the frequency $(\gamma_L \sim k v_{th})$, so the initial amplitude must be large (i.e., $e\phi \sim eE/k \sim m v_{th}^2 = T_e$).

However, we will see that EAW's can be launched by a small amplitude driver if the driver is applied resonantly over many trapping periods. The driver continuously replenishes the energy removed by Landau damping, so the trapped particle distribution (and the EAW) is eventually produced. This result will be demonstrated using a particle in cell (PIC) simulation [5]. For the case where the wavelength is the longest wavelength that fits in the plasma and the plasma is nearly collisionless, the launched EAW persists at nearly constant amplitude long after the driver is turned off.

Stability of the EAW's against decay to other modes is investigated. As mentioned, an EAW with wavelength equal to the length of the plasma rings without decay. However, when this EAW is replicated in space and used as an initial condition for the simulation of a much longer plasma, the EAW is observed to decay to longer wavelength EAW's. In phase space, the trapped particles for an EAW appear to be a vortex structure, and the decay to longer wavelength involves a merger of the vortices [6, 7, 8, 9, 10]. The above results were first reported by the authors in the *Physics of Plasmas* [11].

Evidence suggests that EAW's and the decay of EAW's to longer wavelength were observed in recent experiments using a pure electron plasma column in a Penning trap (see paper by Kabantsev, Valentini and Driscoll in this proceeding). We will discuss the theory of EAW's on such a plasma.

Our simulation results are complementary to recent results reported by Afeyan, Won, Savchenko, Johnson, Ghizzo, and Bertrand [12]. These authors also carry out numerical simulations of nonlinear waves launched by a driver in an unmagnetized plasma. Motivated by suggestions that EAW's might be launched in laser-plasma interaction experiments [13], Afeyan *et al.* focused on relatively large driver amplitudes. They found novel nonlinear waves that they call "Kinetic Electrostatic Electron Nonlinear (KEEN) Waves." These waves are comprised of 4 or 5 significant harmonics, persist only when driven hard enough, and are driven by a wide range of frequencies. In contrast to our work, these authors reported that low amplitude drive does *not* produce coherent EAWs, presumably because the drive was not applied resonantly for a long enough time. We will see that the resonance is relatively narrow and can easily be missed.

DISPERSION RELATIONS

For convenience, we scale time by the inverse plasma frequency ω_p^{-1}, where $\omega_p = \sqrt{4\pi n e^2/m}$ and n is the electron density. Length is scaled by the Debye length $\lambda_D = v_{th}/\omega_p$. With these choices, velocity is scaled by the electron thermal velocity $\lambda_D \omega_p = v_{th}$ and electric field by $\sqrt{4\pi n m v_{th}^2}$.

Using these scalings, the Landau dispersion relation takes the form [2]

$$k^2 = \int_L dv \frac{\partial f_0/\partial v_z}{v - \omega/k} = 0, \tag{1}$$

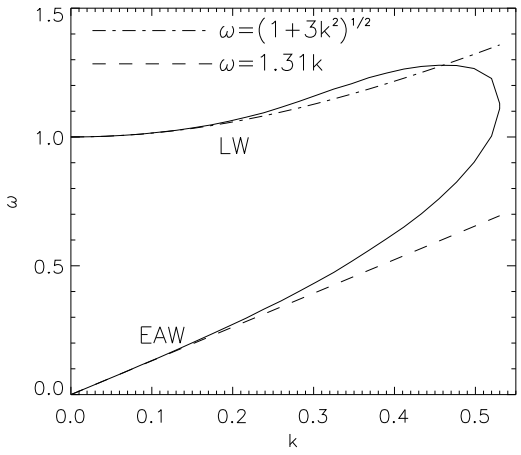

FIGURE 1. The "thumb" dispersion relation. The frequency is expressed in units of the electron plasma frequency and the wave number in units of the inverse of the electron Debye length.

where ω is the complex frequency, k the wave number, and $f_0(v)$ the distribution of electron velocity components in the direction of wave propagation. Here, we take this distribution to be Maxwellian, $f_0(v) = \exp[-v^2/2]/\sqrt{2\pi}$. The subscript L on the integral sign indicates that the velocity integral is to be taken along the Landau contour, dropping down around the pole at $v = \omega/k$. For the high frequency modes of interest, the ions don't participate; throughout the paper the ions are taken to be a uniform neutralizing background charge.

For sufficiently weak damping, the velocity integral along the Landau contour can be approximated by

$$\int_L dv \frac{\partial f_0/\partial v}{v-\omega/k} = P\int_{-\infty}^{+\infty} dv \frac{\partial f_0/\partial v}{v-\omega/k} + \pi i \frac{\partial f_0}{\partial v}\bigg|_{\frac{\omega}{k}}, \tag{2}$$

where P indicates that the principal value is to be taken. As mentioned earlier, the trapped particle distribution for an EAW effectively makes the distribution flat at the wave phase velocity (i.e., $\partial f_0/\partial v|_{\omega/k} \simeq 0$). Thus, Holloway and Dorning [1] obtain a dispersion relation for small amplitude EAWs by retaining only the principal part in the velocity integral of Eq. (1).

Solving for the roots of the resulting dispersion relation then yields the solid curve in Fig. 1. This so-called "thumb" dispersion curve exhibits two roots for small k. The upper root [$\omega = (1+3k^2)^{1/2}$] is the LW and the lower root ($\omega = 1.31k$) is the EAW.

We emphasize that Fig. 1 describes only small amplitude EAWs. Using a Maxwellian distribution for $f_0(v)$ and taking the principal value in the velocity integral assumes that the width of the plateau where $\partial f_0/\partial v = 0$ is infinitesimal. For a finite amplitude EAW, the plateau width is the velocity range over which electrons are trapped in the wave troughs, that is Δv_t, where $(\Delta v_t)^2 \sim E/k$. An infinitesimal trapping width corresponds to an infinitesimal wave amplitude. We will see that the phase velocity for a large amplitude EAW is shifted upward from the value indicated in Fig. 1.

PARTICLE IN CELL SIMULATIONS

Excitation of the EAWs

The PIC simulation follows the electron dynamics in the x-direction, which is the direction of wave propagation. The electron phase space domain for the simulation is $D = [0, L_x] \times [-v_{max}, v_{max}]$, where $v_{max} = 5$. For an initial set of simulations, we choose $L_x = 2\pi/k = 20$, but in later simulations the plasma length is increased to $L_x = 40$ and $L_x = 80$. This increase in length allows for decay to longer wave length EAWs. The time step is $\Delta t = 0.1$. The simulations follow the evolution of $N \sim 5 \times 10^6$ to 10^7 electrons for many plasma periods ($t_{max} = 4000$). The initial electron velocity distribution is taken to be Maxwellian. Periodic boundary conditions in physical space are imposed, and Poisson's equation is solved using a standard Fast Fourier Transform (FFT) routine. The external driver electric field is taken to be of the form

$$E_D(x,t) = E_D^{max}\left[1 + \left(\frac{t-\tau}{\Delta\tau}\right)^n\right]^{-1} \sin(kx - \omega t) \tag{3}$$

where $E_D^{max} = 0.01$, $\tau = 1200$, $\Delta\tau = 600$, $n = 10$, and $k = \pi/10$. The plasma response is studied as a function of the driver frequency ω, or equivalently, phase velocity $v_\phi = \omega/k = 10\omega/\pi$. An abrupt turn on (or off) of the driver field would excite LWs as well as EAWs, complicating the analysis. Thus, the driver is turned on and off adiabatically. The driver amplitude is near E_D^{max} (within a factor of two) for several trapping periods ($t_{\rm off} - t_{\rm on} \simeq 1200 \simeq 11\tau_D$), and is near zero again by $t_{off} = 2000$. Here, the trapping period associated with the maximum driver field is $\tau_D = 2\pi/\sqrt{kE_D^{max}} = 112$.

Figure 2 shows the evolution of the plasma electric field, $E_k(t)$, for two different values of the driver phase velocity. In the top graph (for $v_\phi = 0.4$), $E_k(t)$ rises to a small value while the driver is on, but falls to zero when the driver is turned off. The time t_{off} is indicated by the dashed line. In the bottom graph (for $v_\phi = 1.70$), $E_k(t)$ grows to large amplitude and maintains this amplitude (rings) after the driver is turned off.

Repeating such simulations for many different phase velocities (but holding the other driver parameters fixed at the values listed) yields the peaked graph in Fig. 3. Here, the ordinate is the amplitude of the oscillating plasma electric field at the end of the simulation (long after the driver has been turned off), and the abscissa is the driver phase velocity. For this set of driver parameters, an EAW is driven resonantly for phase velocity $v_\phi \simeq 1.70$.

For the wave number $k = \pi/10$, Fig. 1 implies the resonant phase velocity $v_\phi \simeq 1.45$. However, we must remember that Fig. 1 applies only to small amplitude (infinitesimal) EAWs. For the relatively large EAW in the simulation, the resonant phase velocity is shifted up to 1.70 by the finite plateau width. A separate calculation taking into account a plateau width corresponding to the saturated field amplitude ($E_k^{sat} \simeq .055$) yields the phase velocity $v_\phi \simeq 1.74$.

More precisely, we show that the distribution function obtained in the simulation is effectively a BKG structure. Then we use the BGK formalism to get the EAW solution. Figure 4 shows a false color contour plot of the electron distribution, $f(x,v)$, at the end of the run ($t = 4000$). The color code assigns higher values of f to longer wavelengths in

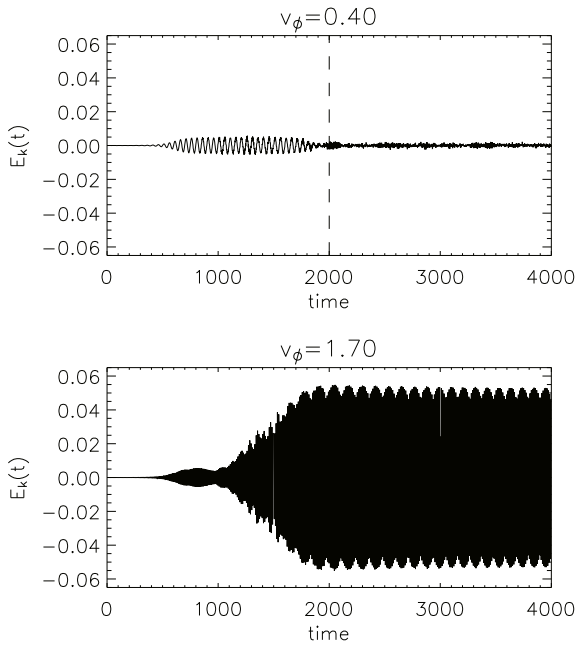

FIGURE 2. Plasma response for two different values of the driver phase velocity: $v_\phi = 0.4$ (at the top) and $v_\phi = 1.70$ (at the bottom).

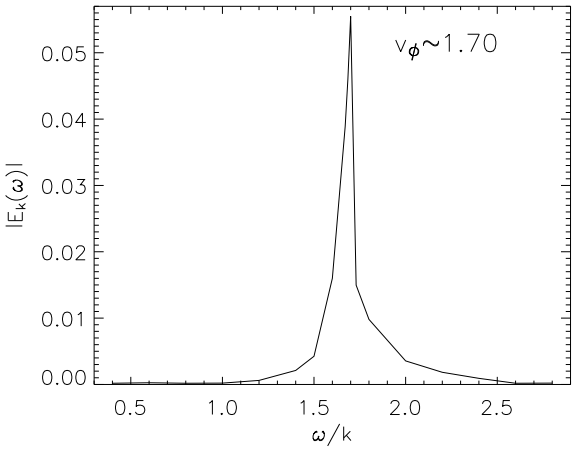

FIGURE 3. The peak of resonance for the EAW.

spectrum. The vortex-like structure in Fig. 4 represents trapped particles, and as expected these particles have a mean velocity equal to the phase velocity $v = 1.7$. The velocity width of the trapped particle region is about $\Delta v_t \simeq 1.7$, which is in agreement with the theoretical expectation $\Delta v_t = 2\sqrt{2E^{\rm sat}/k} = 1.674$. Here, the saturation amplitude of the electric field is $E^{\rm sat} = 2E_k^{\rm sat} \simeq 0.11$ (see bottom graph in Fig. 2). In Fig. 5, we plot the distribution function f at the end of the run as a function of the energy in the wave

frame $\varepsilon = (v - v_\phi)^2/2 - \phi(x, t_{max})$. That is, for each (x, v) in the simulation domain, we plot $f(x, v)$ versus $\varepsilon(x, v)$, resulting in the single curve shown in Fig. 5. This shows that the electron distribution f is a function of the energy ε alone, as expected for a BGK distribution. By using this distribution in the BGK formalism [3] for the phase velocity $v_\phi = 1.7$ and the electric potential amplitude $E^{sat}/k \simeq 0.35$, we get a sinusoidal solution whose wavelength is $\lambda_{BGK} \simeq 19.5$, which is very close to the wavelength of the electric perturbation in the simulation ($\lambda = 20$).

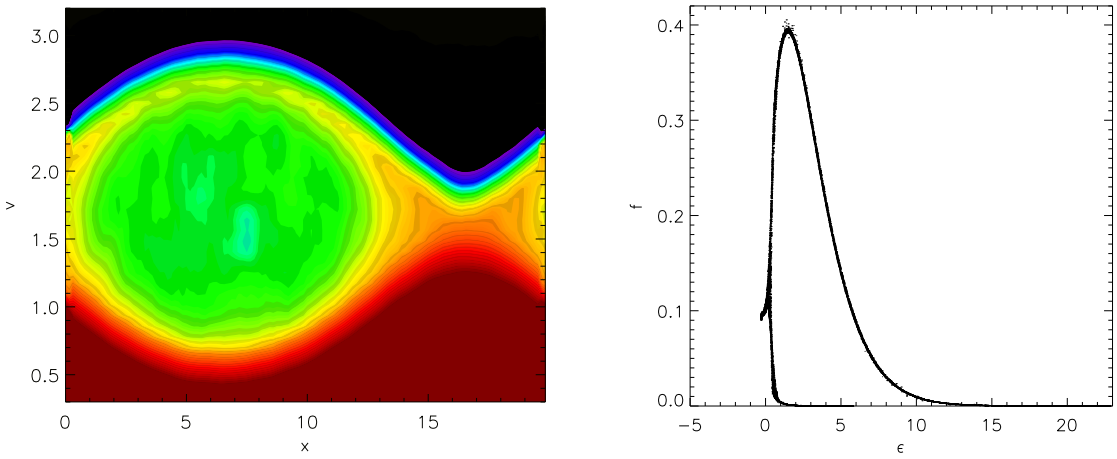

FIGURE 4. The phase space contour plot of the distribution function f at $t = 4000$.

FIGURE 5. The distribution function f plotted as a function of the energy in the wave frame $\varepsilon = (v - v_\phi)^2/2 - \phi(x, t_{max})$.

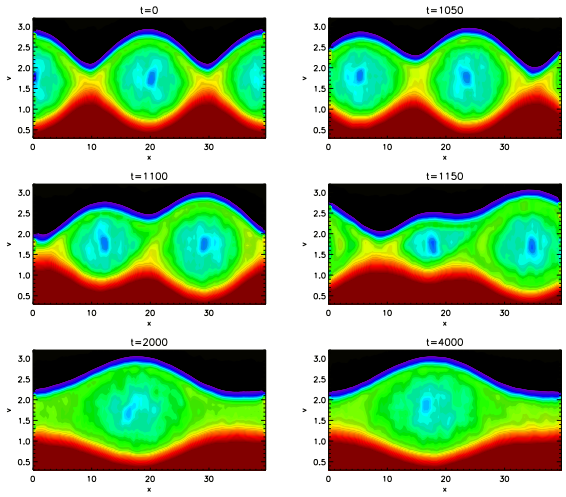

FIGURE 6. The coalescence and merging of two phase space holes.

Decay instability

The EAW in the bottom graph of Fig. 2 rings at nearly constant amplitude after the driver is turned off. However, the wavelength for this mode is the longest wavelength that fits in the simulation domain, so the constant amplitude is no guarantee against decay to a longer wavelength mode. Moreover, previous theory suggested that BGK modes with trapped particles may be subject to such decay instabilities [6, 7, 8, 9, 10].

To investigate the possibility of decay to a longer wavelength mode, we replicate the mode periodically in space and use it as the initial condition for a simulation in a longer domain. The matching from wavelength to wavelength is smooth since periodic boundary conditions were used in the initial simulation.

Figure 6 shows a temporal sequence of phase space contours for the case where the simulation domain has been doubled in length ($L_x = 20 \rightarrow L_x = 40$). The contour plot for $t = 0$ is simply two copies of the plot in Fig. 4 placed side by side. The $t = 0$ plot shows two vortex-like structures representing trapped particles. The sequence of plots shows a progressive merger of the two vortices until there is only a single vortex at $t = 4000$. A decay instability has transferred the energy from mode 2 (i.e., $k = 2 \cdot 2\pi/40 = \pi/10$), to mode 1 (i.e., $k = 1 \cdot 2\pi/40 = \pi/20$); that is, to the longest wavelength that fits in the simulation domain. Also, we have carried out simulations for $L_x = 80$ (4 initial vortices) and again observed merger to a single vortex.

From these observations, we expect that merger to a single vortex (or decay to the longest mode) is a general tendency for EAWs. This is consistent with observations for the merger of phase space vortices in other situations, such as the vortical holes that result from the two stream instability [6, 7, 8, 9, 10].

EAW'S IN A NONNEUTRAL PLASMA

Consider a long pure electron plasma column in a strong uniform axial magnetic field. Let (r, θ, z) be a cylindrical coordinate system with the z-axis coincident with the center line of the column. For simplicity we take the equilibrium distribution of electrons to be of the form $f_0(r, v_z) = n_0(r) f_0(v_z/v_{\rm th})$, where

$$n_0(r) = \begin{cases} n_0 & \text{for} \quad r < R_p \\ 0 & \text{for} \quad R_p < r < R_w \end{cases} \tag{4}$$

is a top-hat radial density profile and $f_0(v_z/v_{\rm th})$ is a Maxwellian. Here, R_p is the radius of the plasma column and R_w is the radius of the conducting cylindrical wall that bounds the confinement region. Because of the large axial magnetic field, only the velocity component v_z enters the dynamics and need be retained in the distribution function. For an electrostatic mode with no azimuthal dependence, the dispersion relation reduces to the simple form [14]

$$k^2 = \omega_p^2 P \int dv_z \frac{\partial f_0/\partial v_z}{\frac{-\omega}{k_z} + v_z}, \tag{5}$$

where k_z is the axial wave number, $K_\perp(k_z)$ an effective transverse (radial) wave number, and $k^2 = k_z^2 + K_\perp^2$. Following the Holloway-Dorning prescription [1], we have replaced

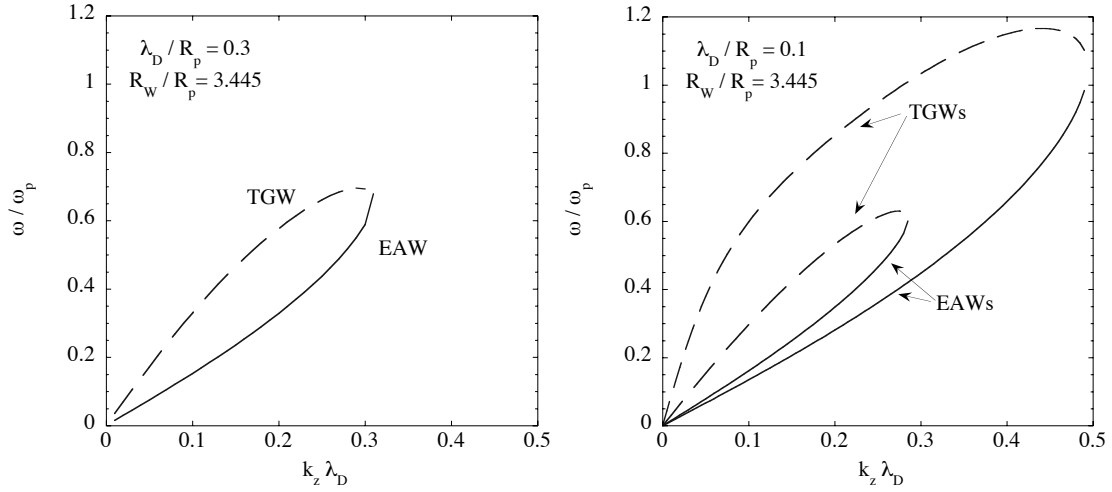

FIGURE 7. Dispersion curves for electron acoustic and Trivelpiece-Gould waves in cylindrical plasmas with top-hat density profiles for which $R_w/R_p = 3.45$ and (a) $\lambda_D/R_p = 0.3$; (b) $\lambda_D/R_p = 0.1$.

the Landau velocity integral by a principal value integral. Note that this dispersion relation differs from that for the 1-D case [see Eq. (4)] only by inclusion of $K_\perp^2$ in the definition of $k^2 = k_z^2 + K_\perp^2$.

For the top hat density profile, the allowed values of $K_\perp(k_z)$ are determined by the equation

$$\frac{R_p K_\perp J_0'(K_\perp R_p)}{J_0(K_\perp R_p)} = k_z R_p \left[\frac{I_0'(k_z R_p)K_0(k_z R_w) - K_0'(k_z R_p)I_0(k_z R_w)}{I_0(k_z R_p)K_0(k_z R_w) - K_0(k_z R_p)I_0(k_z R_w)}\right] \tag{6}$$

where $J_0(x)$, $I_0(x)$, and $K_0(x)$ are Bessel functions. Equation (6) admits a sequence of solutions: $K_\perp^j(k_z)$, where the different solutions corresponding to different radial eigenfunctions of the mode potential. When the solutions are ordered in j so that increasing j corresponds to increasing $K_\perp^j(k_z)$, the $j = 1$ eigenfunction has no nodes in the plasma, the $j = 2$ eigenfunction has a single node in the plasma, and so on.

Each solution for $K_\perp^j(k_z)$ is substituted into the left hand side of Eq. (5), and the resulting equation is solved (when the solution exists) to find the dispersion curve $\omega = \omega^j(k_z)$. When ω is scaled by ω_p and k_z by $\lambda_D^{-1} = \omega_p/v_{th}$, the dispersion curves depend parametrically only on the ratios R_w/R_p and λ_D/R_p.

For the experiments mentioned in the introduction, the density profile $n_0(r)$ is not a top-hat profile with a precise value of R_p, but a reasonable choice for R_p yields the value $R_w/R_p = 3.45$. To illustrate an important dependence on Debye length, we evaluate the dispersion curves for $\lambda_D/R_p = 0.3$ and $\lambda_D/R_p = 0.1$.

Figure 7(a) shows the single dispersion curve $(j = 1)$ found for $\lambda_D/R_p = 0.3$, and Fig. 7(b) shows the two curves ($j = 1$ and $j = 2$) found for $\lambda_D/R_p = 0.1$. As the temperature (and λ_D) increase, dispersion curves shrink and eventually vanish into the origin. This result is easily understandable from Eqs. (5) and (6). One can show that the maximum value of the right hand side of Eq. (5) is $(0.28)/\lambda_D^2$ and that the minimum

value of the left hand side is $[K_\perp^j(0)]^2$. Consequently, a solution for the jth mode is possible only if $[K_\perp^j(0)\lambda_D]^2 < 0.28$. To relate this criterion to Figs. 7(a) and 7(b), we note from Eq. (6) that $K_\perp^1(0) = 1.15/R_p$, $K_\perp^2(0) = 4.03/R_p$, and $K_\perp^3(0) = 7.13/R_p$. Consequently, the dispersion curve exists for $j = 1$ when $\lambda_D/R_p < 0.46$, for $j = 2$ when $\lambda_D/R_p < 0.131$, and for $j = 3$ when $\lambda_D/R_p < 0.0742$. Thus, Fig. 7(a) can have only the $j = 1$ curve and Fig. 7(b) only the $j = 1$ and $j = 2$ curves.

By comparing Fig. 1 and Fig. 7(a), one sees that the "thumb" dispersion curve has become a "finger" dispersion curve. Both the LW (upper curve) and the EAW (lower curve) are acoustic in nature for small k_z. The acoustic nature of the LW for a finite radius plasma is well known; in the acoustic regime the LW is called a Trivelpiece-Gould wave (TGW) [14].

In the limit of small $k^2\lambda_D^2$ approximate dispersion relations are easily obtained for both the TGW and the EAW. From Eq. (5), we see that $k^2\lambda_D^2 \ll 1$ requires that

$$P\int_{-\infty}^{+\infty} \frac{x e^{-x^2/2}}{\frac{\omega}{k_z v_{th}} - x} \ll 1. \tag{7}$$

A zero of the principal value integral occurs for $\omega/k_z v_{th} = 1.31$ which is the EAW dispersion relation, unchanged from the 1-D case. The integral also is small for large $\omega/k_z v_{th}$, varying as $(kV_{th}/\omega)^2$; this limit yields the dispersion relation for TGW's $\omega^j(k_z) = \omega_p k_z/K_\perp^j(0)$. For example, for $j = 1$ the value $K_\perp^1(0) = 1.15/R_p$ implies the TGW dispersion relation $\omega^1 = k_z R_p \omega_p/(1.15)$. Note that the frequency is determined by the plasma line density (i.e., $R_p\omega_p \propto \sqrt{\pi R_p^2 n_0}$).

Qualitatively, the EAW frequency is proportional to the square root of the plasma temperature and is insensitive to the plasma density; whereas, the TGW frequency is proportional to the square root of the line density and is insensitive to the temperature.

In the experiments mentioned in the introduction, the plasma density profile (and, therefore, the line density) was well determined, so TGW's could be identified through accurate ($\sim 1\%$) comparison of measured and predicted frequency. The plasma temperature was not well characterized, so identification of the EAW through a precise check of the measured and predicted frequency was not possible. However, the frequency of the candidate EAW was in a range consistent with the expected plasma temperature, increased as expected with temperature, and was insensitive to plasma line density. Also, the wave exhibited decay to long wave length.

ACKNOWLEDGMENTS

The authors gratefully acknowledge useful discussions with J. J. Dorning, C.F. Driscoll, A.A. Kabantsev, and R.W. Gould. This work was supported by Fondazione Angelo Della Riccia, Firenze (Italy), Center of Excellence for High Performance Computing, Cosenza (Italy), and the National Science Foundation, Grant PHY0354979 (USA).

REFERENCES

1. J. P. Holloway and J. J. Dorning, *Phys. Rev. A* **44**, 3856 (1991).
2. L. D. Landau, *J. Phys. (Moscow)* **10**, 25 (1946).
3. I. B. Bernstein, J. M. Green and M. D. Kruskal, *Phys. Rev. Lett.* **108**, 546 (1957).
4. T. O'Neil, *Phys. Fluids* **8**, 2255 (1965).
5. *Plasma Physics via Computer Simulation*, C. K. Birdsall and A. B. Langdon, McGraw-Hill Book Co., Singapore, 1985.
6. H .L. Berk, C. E. Nielsen, and K. V. Roberts, *Phys. Fluids* **13**, 980 (1970).
7. A. Ghizzo, B. Izrar, P. Bertrand, E. Fijalkov, M. R. Feix, and M. Shoucri, *Phys. Fluids* **31**, 72 (1988).
8. G. Manfredi and P. Bertrand, *Phys. Plasmas* **7**, 2425 (2000).
9. D. C. DePackh, *J. Electron. Control* **13**, 417 (1962).
10. R. A. Dory, *J. Nucl. Energy, Pt. C* **6**, 511 (1964).
11. F. Valentini, T.M. O'Neil and D.H.E. Dubin, *Phys. Plasmas* **13**, 052303 (2006).
12. B. Afeyan, K. Won, V. Savchenko, T. W. Johntson, A. Ghizzo, and P. Bertrand, *Third Biannual IFSA Conference*, Monterey, CA (USA), 2003.
13. D. S. Montgomery, R. J. Focia, H. A. Rose, D. A. Russell, J. A. Cobble, J. C. Fernandez, and R. P. Johnson, Phys. Rev. Lett. **87**, 155001-1 (2001).
14. R. C. Davidson, *Physics of Nonneutral Plasmas*, Imperial College Press and World Scientific, 2001.